A long-range attraction between aggregating 3T3 cells mediated by near-infrared light scattering

Guenter Albrecht-Buehler*

Department of Cell and Molecular Biology, Feinberg School of Medicine, Northwestern University, Chicago, IL 60611

Edited by Judah Folkman, Harvard Medical School, Boston, MA, and approved February 25, 2005 (received for review October 19, 2004)

At what range can a mammalian cell sense the presence of another cell and through what medium? To approach these questions, the formation of aggregates of a 3T3 cell variant ($3T3_x$ cells) grown on solid substrates was studied. Each of the aggregates consisted of cells that, at the time of their seeding, were single and located randomly. Yet somehow they seemed to detect each other within a certain range (R_a) and move together to form aggregates. The article describes a simple assay to measure the value of R_a. When applied to $3T3_x$ cells with altered intensities of near-infrared light scattering (I_{sc}) the assay showed that (*i*) R_a was much larger than one cell diameter, and (*ii*) R_a was directly related to I_{sc}. The results suggest that near-infrared light scattering by the cells mediate a long-range attraction between them, which does not require physical contact and enables them to detect each other's presence.

aggregation | cell sorting

Examining a spontaneous 3T3 cell variant ($3T3_x$ cells) that formed aggregates on solid substrates led to an unexpected observation: When stained with LysoTracker, the cells at the center of each aggregate appeared unusually rich in lysosomes (Fig. 1 *a* and *b*). Conceivably, lysosome production was turned on for unknown reasons in cells that happened to lie at the centers of aggregates. However, in view of my previous work (1–4), it seemed also possible that lysosome-rich cells attracted others by their enhanced ability to scatter near-infrared light. Indeed, the light scattering centers of live mammalian cells are predominantly lysosomes and other perinuclear organelles, such as peroxisomes and mitochondria (Fig. 1 *c* and *d*).

To test whether the more intensely light-scattering cells (hyperscattering cells) would become centers of aggregation, I allowed $3T3_x$ cells to ingest particles in the range of 0.1–3.0 μm in diameter. These particles were similar in size and shape to normal perinuclear granules but scattered considerably more light (Fig. 1*e*). Inert latex and synthetic diamond particles were used because they have no known chemical effect on the genome, membrane, or cytoplasm of the cells. Indeed, the centers of the aggregates formed by such hyperscattering cells were the richest in ingested particles and scattered the most light (Fig. 1 *f* and *g*).

These observations suggested a characteristic quantity for all cells that were able to aggregate on solid substrates, namely their range of aggregation, R_a. R_a may be defined as the distance at which randomly plated cells are able to detect each other and move together to form aggregates.

Measuring R_a quantitatively and accurately would offer the opportunity to answer two very fundamental questions about aggregating mammalian cells. First, is R_a considerably larger than one cell diameter (i.e., is there a long-range attraction between them)? Second, does R_a depend on the near-infrared light scattering intensity (I_{sc}) of the cells (i.e., is near-infrared light a mediator for the long-range attraction)?

The present article describes a simple method to measure R_a. When applied to hyperscattering cells, it led to the conclusion that R_a is considerably larger than one cell diameter and that it depends on I_{sc}.

Please note that all but two of the experiments described below excluded visible light from reaching the cells inside the culture incubators. Therefore, the best candidate for light scattered by the experimental cells was the near-infrared portion of the so-called black-body radiation, i.e., the heat radiation corresponding to the ambient temperature of 37°C (see *Discussion*).

Materials and Methods

Cell Culture. $3T3_x$ cells were a spontaneous variant derived from normal Swiss 3T3 cells (a gift of Howard Green, Harvard Medical School, Boston) by growing the cells in DMEM with 10% FCS for >40 passages without subcloning. The cells were split 1:3 and grown in DMEM with 10% of normal calf serum thereafter.

Particles and Particle Suspensions. Latex particles were purchased from Polysciences (Warrington, PA), and 1.00-μm Polycrystalline diamond particles (catalog no. SSX 0.75–1.25) were purchased from L. M. Van Moppes (Geneva). A second kind of diamond particle (catalog no. PCD-F 0–2μ) was purchased from Engis (Wheeling, IL). The first kind of diamond particle appeared dark gray, whereas the second appeared white as a result of their different method of catalysis. Both types had a very narrow size range, and their shape was regular and crystalline. All particles were kept in an aqueous suspension of 2.5% solids. The suspension of diamond particles was sonicated before every use.

Preparation of Hyperscattering Cells. Volumes between 20 and 200 μl of the particle suspensions were added to 8 ml of culture medium in 10-cm culture dishes. Three-day-old $3T3_x$ cells were trypsinized, and 2×10^6 cells were added to the particle-containing dish. After 2–3 days, the particle-loaded cells were harvested by trypsinization, pelleted in a tabletop centrifuge, and resuspended in normal culture medium by vigorous pipetting.

Measurement of Light Scattering of Hyperscattering Cells. Samples of the cell suspensions used in the experiments were diluted to final concentrations of 2×10^5 cells per ml, placed in cuvettes, and irradiated from the side by the beam of a 830-nm gallium aluminum–arsenide laser with a peak intensity of 40 mW (GALA Laser system, DO Industries, Rochester, NY). A fiber-optics cable at right angles to the beam fed the scattered light into a near-infrared-sensitive photomultiplier setup (Hamamatsu Photonics, Bridgewater, NJ) whose current was read on an oscilloscope.

Lysosome and Nuclear Staining. For lysosome staining, LysoTracker red DND-99 (Molecular Probes) was added to the fixed cells of a culture dish to yield a final concentration of 100 nM. For nuclear staining, 3 μM Hoechst stain was added. Subsequently, a coverslip was placed over the preparation, and the

This paper was submitted directly (Track II) to the PNAS office.

Freely available online through the PNAS open access option.

*E-mail: g-buehler@northwestern.edu.

www.pnas.org/cgi/doi/10.1073/pnas.0407763102

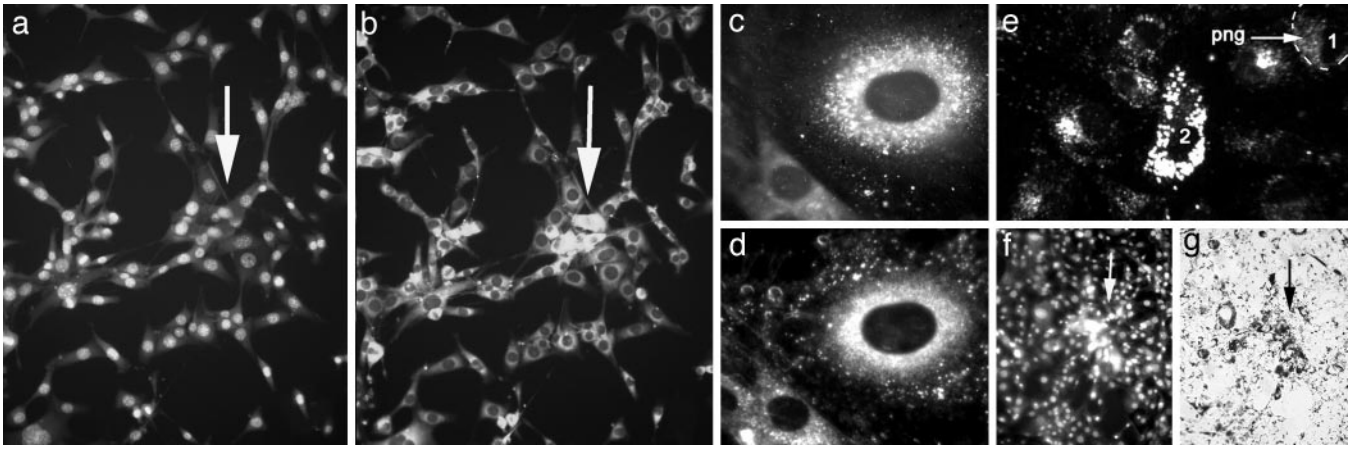

Fig. 1. Heuristics for a possible linkage between light scattering and aggregation. (*a*) Appearance of a typical aggregate of $3T3_x$ cells (arrow) whose nuclei are stained with Hoechst dye. (*b*) The same aggregate stained with LysoTracker reveals that lysosome-rich cells are located at the center of the aggregate. (*c*) Lysosome staining of a 3T3 cell. (*d*) Darkfield micrograph of the same cell suggesting that the light-scattering centers of the cell contain the lysosomes. The dark ovals in *c* and *d* are the nuclei given that they do not scatter light and do not contain lysosomes. (*e*) Darkfield micrograph of a hyperscattering $3T3_x$ (labeled 2) cell that was formed by the ingestion of strongly light-scattering, 1-μm, latex particles. The cell is surrounded by particle-free $3T3_x$ cells (e.g., labeled 1) whose perinuclear granules (png) scatter much less light than the hyperscattering cell. (*f*) Hoechst staining of an aggregate of hyperscattering cells. (*g*) Brightfield micrograph of the same aggregate. The cells with the most ingested particles that appear the darkest because they scatter the most light are located at the center of the aggregate.

cells were photographed while both stains stayed in the immersion medium.

Test Substrates for Unidirectional Aggregation. The bottom of a 6-cm culture dish was coated with a 1- to 2-mm thin layer of Sylgard 184 (Dow–Corning) and polymerized for 1 h at 55°C, generating a sterile surface that was essentially nonadhesive for cells. Subsequently, the surface was rendered adhesive by the vacuum evaporation of a thin, transparent film (≈50% light extinction) of NiCr (see ref. 2) except in areas that were masked by five electron microscope grids (diameter, 3 mm) placed randomly on the Sylgard 184 surface before the evaporation. The copper electron microscope grids (model no. G300P-Cu, EMS, Port Washington, PA) had a parallel bar pattern to produce parallel strips of alternating adhesive and nonadhesive areas. For the experiments, $\approx 1.5 \times 10^6$ particle-containing cells were plated into 6 ml of culture medium of the test substrates that were fixed and examined 2 days later.

Microscopy. With kind permission of Lester Binder (Northwestern University, Chicago, IL) the experimental cells were photographed with his Nikon Eclipse E800 microscope (Fryer, Huntley, IL) with attached Spot Camera (Diagnostic Instruments, Sterling Heights, MI).

Time-Lapse Observations. Cells in 35-mm dishes were mounted in an airtight chamber, placed on an inverted Leitz microscope at 37°C, and photographed every 15 min for 2–3 days with a digital camera (EDC-1000HR, Electrim, Princeton, NJ) and custom software (available upon request).

Results

Near-Infrared Light Scattering of Hyperscattering Cells. The average I_{sc} of hyperscattering cells at 830 nm was measured as described in *Materials and Methods* and was found to depend on the material, size, and concentration of the ingested particles. As shown in the example of Fig. 2, the I_{sc} of hyperscattering cells that had ingested different amounts and kinds of particles exceeded the light scattering of $3T3_x$ cells in an adjustable way by as much as 175-fold.

Time-lapse observations of the ingested particles demonstrated their incessant motion indistinguishable from that of normal perinuclear particles. This motion caused stochastic clustering of the particles which, in turn, generated continuous fluctuations of I_{sc}.

Aggregation of Hyperscattering Cells. Aggregating cells are commonly thought to adhere to one another after accidental collisions, analogous to molecules precipitating out of solution. In contrast, time-lapse observations of the aggregation behavior of hyperscattering cells mixed with particle-free $3T3_x$ cells demonstrated a very different process (Fig. 3).

After the hyperscattering cells had settled randomly and spread (Fig. 3*a*), they moved around while drawing closer to each other as if attracted by a mutual, long-range attraction. In the course of the next 2 days, they continued to narrow the distances between them. Eventually, the continuous cell growth (arrows in Fig. 3*b*) increased the overall cell density and reduced their free movements (Fig. 3*c*) to such a degree that they appeared trapped

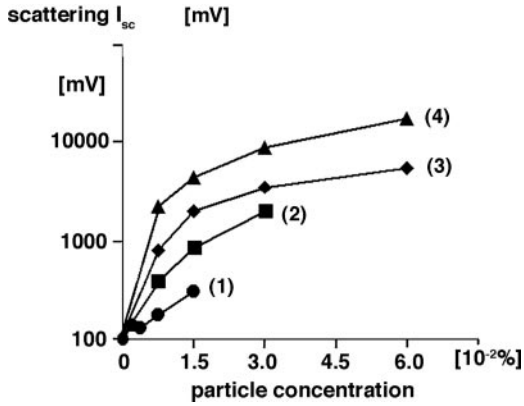

Fig. 2. Standardized light scattering I_{sc} of hyperscattering cells at 830 nm as a function of the concentration (wt/wt) of ingested particles of different materials Line 1, 1-μm latex particles; line 2, 2-μm latex particles; line 3, 1-μm dark diamond particles; line 4, 1-μm white diamond particles. The abscissa of the graph indicates particle concentration, and the ordinate indicates light scattering of particle-loaded cells measured as photomultiplier readings.

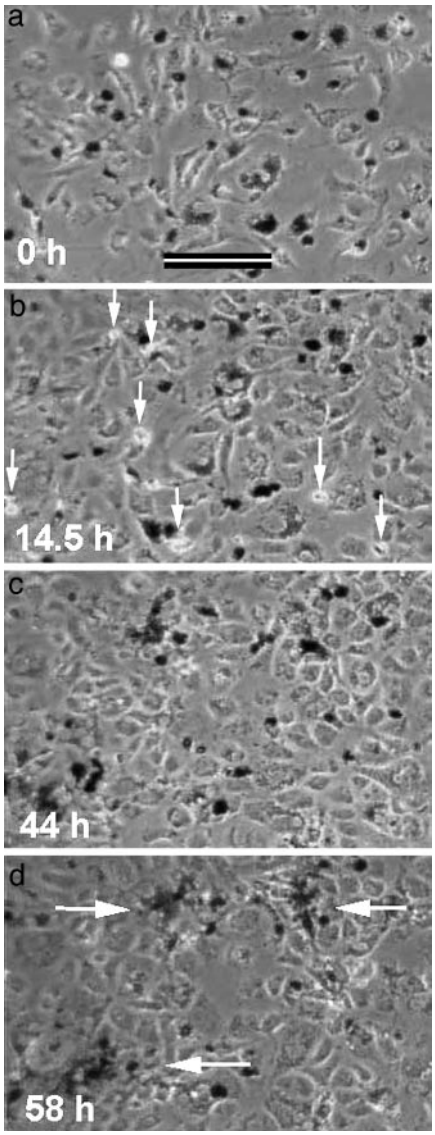

Fig. 3. Time-lapse observation of the aggregation of hyperscattering cells mixed with particle-free $3T3_x$ cells. The hyperscattering cells contained 1-μm latex particles and appear dark in phase contrast (low levels of 600-nm field illumination). White arrows in *b* point to several mitotic figures. White arrows in *d* point to final aggregates. The hyperscattering cells drew closer to each other long before they were able to make physical contact.

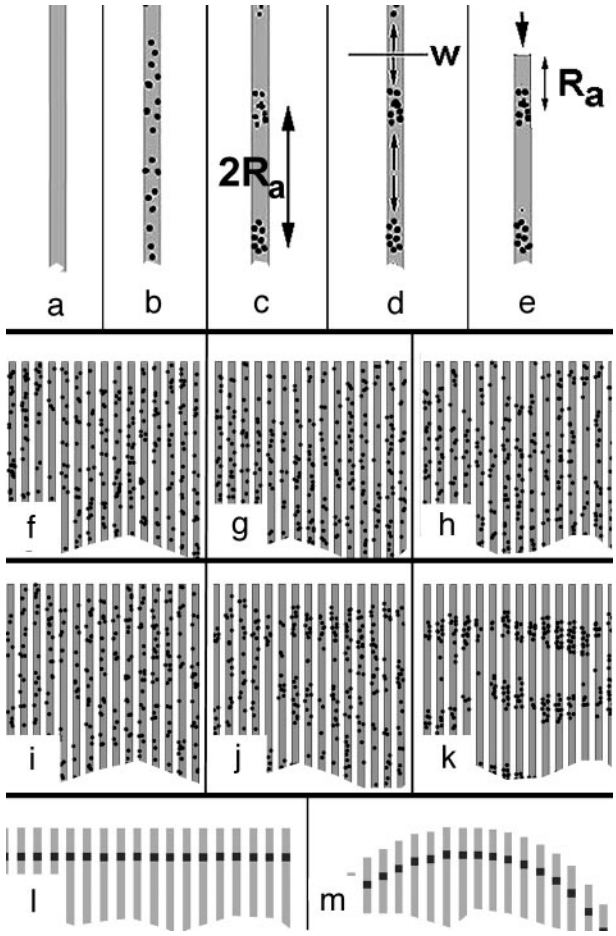

Fig. 4. Assay to measure R_a (unidirectional assay of cell aggregation). (*a–e*) Basic rationale. Different stages of the formation of the outermost aggregate a certain distance R_a away from the end of the strip (see text). (*f–k*) Computer simulation of the formation of the outermost aggregates. [Simulation parameters: cell diameter, 5 pixels; strip width, 15 pixels; rounds of simulation: 0 (*f* and *i*), 40 (*g* and *j*), and 100 (*h* and *k*)]. (*f–h*) $R_a = 0$. No aggregation occurred. (*i–k*) $R_a = 100$. Formation of aggregates at a distance R_a away from the ends of the strips. The distance between aggregates on the same strip is $\approx 2R_a$. (*l*) Predicted locations of the outermost aggregates (dark markings) on an array of parallel strips form a line parallel to the ends if the array is rectangular. (*m*) Predicted locations of the outermost aggregates (dark markings) on an array of parallel strips lie along a circle if the ends form a circle. This particular geometry is used in the present study.

near each other. At that stage, they seemed to touch each other and tighten the aggregates (arrows in Fig. 3*d*).

A Quantitative Assay for R_a (Unidirectional Aggregation). ***Basic rationale.*** In a thought experiment, we assume that randomly plated cells attach and spread on an infinitely long, narrow adhesive strip that is surrounded by a nonadhesive substrate (Fig. 4 *a* and *b*). Subsequently, the cells will migrate up and down the strip while avoiding the nonadhesive surface on either side. If the cells are capable of aggregation, then they will eventually form aggregates at random locations with an average distance of $2R_a$ between them (Fig. 4*c*). The midpoint, *w*, at distances R_a between any two adjacent aggregates may be considered a watershed of cell migration as the cells ahead of or behind this point effectively migrated to opposite sides while forming the aggregates (Fig. 4*d*). Assume that the strip was cut off at such a location *w* (Fig. 4*e*). Cutting the strip would not affect the aggregate behind *w* because the cells ahead of the cut would have migrated in the opposite direction anyway. Therefore, one may conclude that the first aggregate of every strip will be located at a distance of R_a from the end of the strip.

Computer simulations of the described process (program available upon request) confirmed the above conclusions. No aggregates formed when $R_a = 0$ (Fig. 4 *f–h*). In contrast, tight aggregates formed and lined up a distance of R_a away from the ends of the strips, when $R_a \gg$ cell diameter (Fig. 4 *i–k*).

Evidence for a long-range attraction: Aggregation arcs. To apply this rationale, parallel arrays of narrow, adhesive strips on a nonadhesive Sylgard 184 surface by evaporation of thin layers of NiCr. By using readily available 300-mesh electron microscope grids with parallel bar patterns as evaporation masks, parallel arrays of 30 adhesive strips whose ends formed a circle with radius $r =$ 1.25 mm (Fig. 5*a*) were obtained. As a consequence of this particular geometry, all points that were shifted by a distance of R_a away from the ends of each strip must lie along two half circles

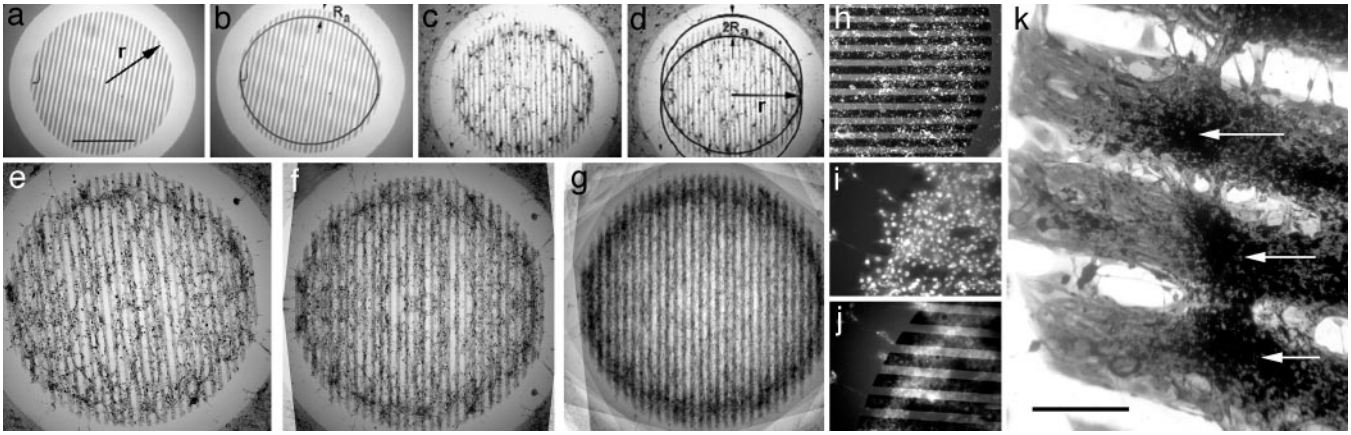

Fig. 5. Unidirectional aggregation of 3T3$_x$ cells. (*a*) Circular pattern of adhesive strips (gray areas) on a nonadhesive substrate (bright areas) generated by evaporating a thin layer of NiCr onto a Sylgard 184 surface with a bar pattern electron microscope grid as a mask (r = 1.25 mm). (Bar, 1 mm.) (*b*) According to the basic rationale, the outermost cell aggregates on each strip must be located a distance R_a away from each end. The two circular arcs indicate these locations. (*c*) Example of aggregates of hyperscattering cells located along the predicted aggregation arcs as seen in brightfield microscopy. (*d*) Quantitative evaluation of the circular aggregation arcs by matching them to two circles of radius r. The shift between the circles is 2R_a. Obviously, R_a is much larger than one cell diameter, suggesting that there is a long-range attraction between the aggregating cells. (*e–g*) Increase of visibility and accuracy of the aggregation arcs by image averaging. (*e*) Unprocessed image. (*f*) Superimposition of *e* with its own mirror image (self-mirrored image). (*g*) Image average of all five test fields of a test substrate, each processed as in *f*. (*h*) Visualization of aggregation arcs in the case of low-level scattering of ingested particles. Arc formation of cells that had ingested 0.1-μm fluorescent latex particles. Even though the particles are too small to be detected in brightfield micrographs, the self-mirrored fluorescence micrograph shows the location of the outermost aggregates away from the ends of the adhesive strips. (*i* and *j*) Visualization of aggregation arcs in the case of particle-free 3T3$_x$ cells. (*i*) Hoechst staining of a field of particle-free cells. (*j*) LysoTracker staining of the same field reveals an aggregation arc formed by lysosome-rich cells. (*k*) Coomassie-blue-stained 3T3$_x$ cells that had formed aggregation arcs on the large and wide-spaced strips derived from a 100-mesh grid during the 5 days after they had ingested white diamond particles. White arrows point to the aggregates of particle-rich cells that constituted parts of the arc. Obviously, the sheet of particle-rich, aggregated cells did not retract under some kind of tension away from the ends of the strip but were embedded in a much larger cell sheet that covered the entire strip. (Bar, 150 μm.)

with the same radius r (Figs. 4*m* and 5*b*). According to the basic rationale (Fig. 4 *b* and *c*), these were the predicted locations of the outermost aggregates of cells (aggregation arcs) whose distance from the ends of each strip could be used to measure R_a.

Indeed, when plated on such substrates, hyperscattering cells aggregated along circular arcs (Fig. 5 *c* and *e*) that were noticeably shifted away from the ends of the strips. Comparing the shift with the width of the strips of 43 μm as a crude scale, it was qualitatively clear that the value of R_a was much larger than the average cell diameter of 22 $\pm$ 5 μm. The latter value was measured in the adhesive areas around the test substrates at the same high cell density that was used in the experiments. The results showed that there was a long-range attraction between the aggregating cells.

The standardized exposure of the cells to particles yielded a rather uniform distribution of particles inside the cells. However, after replating them, the processes of cell divisions and exocytosis of the indigestible particles during the 2 days of the duration of the assay led to considerable diversity. It was this very diversity that helped to increase the contrast between the particle-loaded cells in the aggregation arcs and the other cells that contained relatively fewer particles and covered the strips. In this way, the assay took advantage of a certain degree of nonuniformity of the number of ingested particles.

***Measurement of* R_a.** The actual quantitative measurement of the value of R_a was a simple fitting procedure. Because the radius, r, of the circular aggregation arcs was known, two circles with this radius were superimposed on photographs of the experimental arrays and shifted around until they fit the two aggregation arcs optimally. Measuring the distance, D, between the two circles yielded the desired value: $R_a = D/2$ (Fig. 5*d*). The two circles had to intersect at the poles of the circular pattern of adhesive strips, which served as an internal control for the curve-fitting procedure.

***Image averaging to improve the accuracy of measurements of* R_a.** The visibility of the aggregation arcs could be enhanced by superimposing each original image (Fig. 5*e*) on its own mirror image (Fig. 5*f*). Throughout this study, such "self-mirrored" images were used to determine the values of R_a. Applying this procedure to all five arrays of a test substrate yielded a standard deviation of $\approx$15%. For even better visibility and accuracy, one could superimpose the self-mirrored images of all five arrays of a test substrate. The procedure was equivalent to the optical average of 2 $\times$ 5 = 10 independent experiments (Fig. 5*g*).

Measurement of aggregation arcs at low levels of scattering. When aggregation arcs were no longer visible in brightfield microscopy because the ingested particles were $<$0.5 μm, fluorescent latex particles were used instead. Fig. 5*h* shows the example of an aggregation arc formed by cells that had ingested fluorescent latex particles with a 0.1-μm diameter. As in the case of larger particles, the first cell aggregates were shifted by a distance R_a from the ends of the adhesive strips. However, the distance was visibly shorter than in the case of the strongly light-scattering latex and diamond particles (e.g., Fig. 5 *c* and *e*).

Measurement of aggregation arcs of particle-free cells. It was important to determine the value of R_a also for particle-free 3T3$_x$ cells, because their light scattering resembled that of cells *in vivo*. Measuring R_a in this case took advantage of the initial observation that cell aggregates were centered on lysosome-rich cells. Indeed, as shown in Fig. 5*j*, the cells rich in lysosomes formed aggregation patterns including arcs, even though their cell density, as shown by Hoechst staining of the nuclei, appeared quite uniform (Fig. 5*i*). The aggregation arcs were very close to the end of the strips on the test substrate yielding a value of R_a = 87 $\pm$ 5 μm.

Please note that Fig. 5 *i* and *j* exclude the possibility that aggregation arcs resulted from differential substrate adhesion and some kind of retraction of the cells away from the end of a strip. Obviously, the lysosome-rich cells of the aggregation arc of

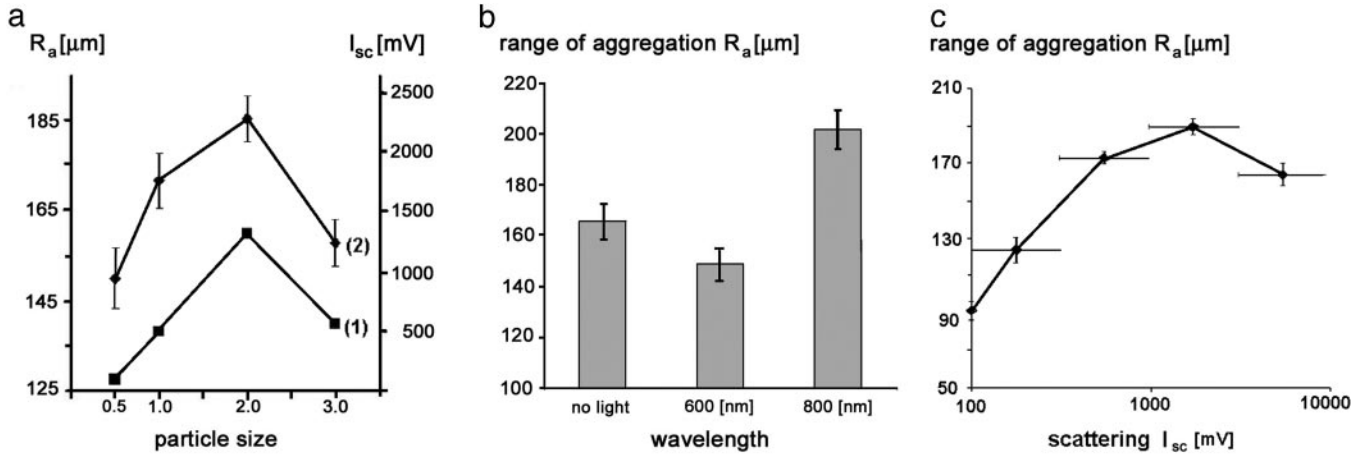

Fig. 6. Quantitation of arc formation. (*a*) Parallels between the I_{sc} of hyperscattering cells at 830 nm (line 1) and the R_a (line 2). The abscissa of the graph indicates the size of the latex particles used to generate the hyperscattering cells. The left-hand ordinate indicates the R_a of hyperscattering cells, and the right-hand ordinate indicates their I_{sc}. Error bars indicate the error of the means of two independent experiments, with 10 measurements per data point. (*b*) Effect of continuous irradiation of hyperscattering cells with 12–15 μW/cm^2 of light at a distance of 45 mm. The columns represent the average of 14 measurements of the R_a in three independent experiments. Error bars indicate the error of the mean. (*c*) Correlation between R_a and I_{sc} of hyperscattering cells. Each data point represents the average of 20–45 individual measurements of R_a. Horizontal error bars indicate the size of the sorting intervals that yielded the indicated averages. Vertical error bars indicate the error of the mean of these averages.

Fig. 5*j* were embedded in a much larger sheet of cells that extended all of the way to the end of the strip. Identical results could be obtained by Coomassie blue staining of preparations that involved particle-loaded cells, such as in Fig. 5*k*. In all cases, the aggregation arcs were parts of cell sheets that extended to the ends of the strips.

Correlation Between I_{sc} and R_a. The above quantitative methods made it possible to approach the two questions raised in the Introduction that concerned the size of R_a and its relationship with the I_{sc} of the cells. Therefore, the R_a values of 3T3$_x$ cells and their hyperscattering derivatives were measured as a function of their near-infrared light scattering in the absence and presence of exogenous light sources.

The results shown in Fig. 6 provide an immediate answer for the first question. These results demonstrate values of R_a between 85 and 247 μm, which are larger than one cell diameter of 22 ± 5 μm. The answer to the second question is suggested by the following three experiments.

Parallels between I_{sc} and R_a. The scattering intensity of hyperscattering cells did not rise monotonously with the size of their ingested particles; it decreased after reaching a peak for 2-μm large particles (Fig. 6*a*, line 1) because the cells ingested fewer of the larger particles. I found that the value of R_a changed in a similar way as a function of particle size (Fig. 6*a*, line 2), suggesting that light scattering may play a role in aggregation.

Influence of irradiation on R_a. Earlier work (1, 2, 4) has shown that 3T3 cells reacted most sensitively to near-infrared light at ≈800 nm if the light source pulsated. Therefore, hyperscattering cells were tested under irradiation with the visible wavelength of 600 ± 10 nm or the near-infrared wavelength of 800 ± 10 nm light at intensities of 12–15 μW/cm^2 perpendicular to the surface of the test substrates. Please note that it was unnecessary to use pulsating light for the irradiation because the light scattered by the stochastically moving perinuclear particles inside the cells was fluctuating and thus pulsating in a natural way.

The averages of three independent experiments and 14 measurements for each data point showed a 10 ± 4% reduction of the value of R_a with visible light, whereas irradiation with the near-infrared wavelength increased the value of R_a by 22 ± 4% (Fig. 6*b*). Such changes of R_a may appear small, but a one-dimensional increase of R_a as small as 26% would effectively double the volume from which three-dimensional aggregates recruit their constituent cells, because $(1.26)^3 = 2$.

Correlation function between R_a and I_{sc}. To determine the correlation function between the light scattering I_{sc} of hyperscattering cells and their range of aggregation R_a, one was plotted against the other. The large range of scattering intensities of hyperscattering cells (see Fig. 2) made it necessary to select intervals that had the same size on a logarithmic scale (horizontal bars in Fig. 6*c*). Grouping 126 individual measurements of R_a into these intervals yielded 10–45 measurements of R_a for each interval. Fig. 6*c* shows the average values of R_a for each interval together with the value of R_a obtained for particle-free cells.

The value of R_a more than doubled as the scattering intensity of the cells increased 18-fold over the value of particle-free cells. This result suggests that the more a cell was able to scatter light, the more likely it was able to be detected by distant cells and, thus, the larger was the distance from which the cells flocked together.

At extremely high scattering intensities, $I_{sc} > 3{,}000$ mV, R_a decreased again. This finding may be explained by an increased speed of aggregation at these intensities, which increased the number of aggregates and, thus, reduced the average R_a between them.

The Range of Aggregation of Other Fibroblasts. Not only 3T3$_x$ cells but also other fibroblasts, such as normal 3T3 cells and baby hamster kidney (BHK) cells, formed aggregation arcs after their conversion to hyperscattering cells. Although the formation took normal 3T3 cells and BHK cells 2–3 times longer than 3T3$_x$ cells, the value of R_a for normal 3T3 cells was the same as for 3T3$_x$ cells. BHK fibroblasts cells formed long, stretched aggregates that generated 28% larger values of R_a than 3T3 cells.

Discussion

The common interpretation of cellular aggregation requires no long-range attraction between cells but only a sufficiently strong adhesive force between like cells to prevent their separation after accidental contacts (5–10). This interpretation certainly applies to the aggregation of cells that are shaken in liquid suspension, where they have no means of locomotion of their own.

In contrast, the present case of the aggregation of cells attached to solid substrates suggested that there is a long-range attraction between the cells: Time-lapse observations showed that the aggregating hyperscattering cells in the initial phases of their aggregation drew closer long before making any physical contact. Moreover, the large size of R_a suggested that the aggregating cells attracted each other over a distance of many cell diameters.

Based on the described relationship between I_{sc} and R_a I propose that the light scattering of perinuclear particles mediated this attraction, which appeared to enable the aggregating cells to detect and move toward the most "visible" cells from a distance of many cell diameters.

Which kind of light could the experimental cells have scattered? With the exception of the experiments described in Figs. 3 and 6*b*, all experiments were carried out in the absence of any visible light inside culture incubators. The only light that was consistently present in all experiments was the black-body radiation corresponding to the ambient temperature of 37°C. It contains no UV or visible light but considerable amounts of infrared light with a peak emission at a wavelength of 15,400 nm (11). The water inside and around the cells absorbs almost all of the infrared light at wavelengths of >1,500 nm (12). Therefore, the only light in the above experiments left for the cells to scatter was in the range of 800–1,500 nm. Previous, independent experiments (1–4) suggest that the range of active wavelengths can be narrowed further to the interval between 800 and 900 nm.

One must keep in mind, although, that the intensity of the scattered light of the black body radiation is extremely small. Therefore, it may turn out that cells are not able to detect the scattered light of any single cell, but need the combined scattering of small groups. Regardless, the method they employ for detection must be extraordinary. Modern single photon detectors and sophisticated data-processing methods including Fourier and wavelet analysis were barely able to detect the scattering of the black-body radiation by small groups of cells (unpublished results). It seems inescapable that cells also employ a highly sophisticated detection and data-processing system that ultimately coordinates all of the actions required for aggregation. Such actions would include adhesion, polarization, cytoskeletal architecture, shape changes, migration, interactions with the extracellular matrix and possibly many more. Because several of these actions are also known to feed back on the genome (e.g., refs. 13–15), the postulated detection and data-processing systems appear capable of essentially influencing actions of the entire cell.

I thank Dr. Howard Green and Dr. Edwin Taylor (Northwestern University) for critically reading the manuscript and for valuable suggestions. This work was supported by Air Force Office of Scientific Research Grant F49620-02-1-0395 and Defense Advanced Research Projects Agency Grant 521402/MDA972-92-C-001.

1. Albrecht-Buehler, G. (1991) *J. Cell Biol.* **114,** 493–502.
2. Albrecht-Buehler, G. (1992) *Proc. Natl. Acad. Sci. USA* **89,** 8288–8292.
3. Albrecht-Buehler, G. (1995) *Cell Motil. Cytoskeleton* **32,** 299–304.
4. Albrecht-Buehler, G. (1998) *Cell Motil. Cytoskeleton* **40,** 183–192.
5. Armstrong, P. B. (1989) *Crit. Rev. Biochem. Mol. Biol.* **24,** 119–149.
6. Holtfreter, J. (1944) *Rev. Can. Biol.* **3,** 220–250.
7. Moscona, A. A. & Moscona, H. (1952) *J. Anat.* **86,** 287–301.
8. Moscona, A. A. (1960) in *Developing Cell Systems and Their Control*, ed. Rudnick, D. (Academic, New York), p. 45–70.
9. Steinberg, M. S. (1963) *Science* **141,** 401–408.
10. Townes, P. & Holtfreter, J. (1955) *J. Exp. Zool.* **128,** 53–120.
11. Planck, M. (1910) *Ann. Phys.* **31,** 758–768.
12. Wolfe, W. L. and Zissis, G. J. (1989) in *The Infrared Handbook* (Environ. Res. Inst. Michigan, Ann Arbor, MI), pp. 3–107.
13. Folkman, J. & Moscona, A. (1978) *Nature* **273,** 345–349.
14. Ingber, D. E. & Folkman, J. (1989) *J. Cell Biol.* **109,** 317–330.
15. Streuli C. H., Bailey, N. & Bissell, M. J. (1991) *J. Cell Biol.* **115,** 1383–1395.